Article:
Wang, A., Fei, M., Du, D. et al. (2025) Scalable Neural Network Control for Nonlinear DC Microgrids Under Plug-and-Play Operations. IEEE Transactions on Industrial Informatics, 21 (5). pp. 3849-3859. ISSN: 1551-3203

https://doi.org/10.1109/tii.2025.3534423

Scalable Neural Network Control for Nonlinear DC Microgrids Under Plug-and-Play Operations

***Abstract*— Plug-and-play (PnP) operations of distributed generation units (DGUs) with constant power loads (CPLs) often destabilize DC microgrids (DCmGs). To address this issue, this paper proposes a scalable neural network control strategy for nonlinear DCmGs with CPLs, enabling seamless PnP operations of DGUs. A radial basis function (RBF) neural network is employed to handle the uncertain CPL nonlinearity without requiring any prior knowledge. A structured Lyapunov matrix is utilized to eliminate the coupling effects of power lines by reshaping them into a Laplacian matrix structure. Within this framework, a scalable neural network control approach is proposed, integrating a nominal controller with explicit gain inequalities and an adaptive controller governed by an adaptation law. This approach operates locally, independent of other DGUs and power lines, ensuring PnP operations and maintaining uniformly ultimately bounded stability. The effectiveness of the proposed method is validated through case studies on a modified IEEE 37-bus test system.**

***Index Terms*— DC microgrids (DCmGs), scalable control, plug-and-play (PnP), constant power loads (CPLs), radial basis function (RBF) neural network.**

I. Introduction

THE on-going energy crises and growing environmental concerns have accelerated the development and adoption of renewable energy sources (RESs), such as photovoltaic panels and wind turbines [1]–[3]. Microgrids have emerged as essential components of modern power systems, providing a sustainable and low-carbon platform for integrating diverse RESs [4]–[6]. They are typically categorized into direct-current microgrids (DCmGs) and alternating-current microgrids (ACmGs), both of which can perform in islanded or grid-connected modes [7]–[9]. DCmGs, in particular, offer notable advantages over ACmGs, including independence from frequency regulation, harmonics cancellation, and reactive power flow [10]. Therefore, DCmGs are widely applied in electric vehicle (EV) charging stations, green building communities, and marine power systems [11].

However, when the distributed generation units (DGUs) integrating RESs are used to meet constant power loads (CPLs) in DCmGs, two issues have to be addressed. 1) *Voltage stabilization under CPLs:* Electronic loads, such as EV chargers and air conditioners, behave as CPLs, introducing nonlinear features and negative impedance effects [12]. These features can destabilize the system, often leading to voltage drifts or even collapse [13]. Consequently, CPLs are considered among the most challenging components in the standard ZIP (constant impedance, constant current, and constant power) load model used in DCmG stability analysis [14]. 2) *Scalability under plug-and-play (PnP) operations:* In practice, some DGUs may need to be temporarily unplugged during low-demand periods to improve system efficiency and reduce costs [15], while additional DGUs must be plugged in during peak demand periods to stabilize voltage under increased loads, such as those imposed by fast EV charging [16]. These PnP operations may induce voltage shocks due to variations in both the number of DGUs and the coupling configuration of power lines [17], [18]. In this context, it is not surprising that DCmG stabilization and scalability have garnered significant attention in recent years.

Voltage stabilization under CPLs can be achieved by addressing their nonlinearities. For example, Hu *et al.* [19] proposed a robust control strategy that models CPL nonlinearity as bounded external disturbances. In [20], Jacobian linearization was employed to analyze eigenvalues in linearized DCmGs with CPLs. A nonlinear backstepping control method was introduced in [21], where the nonlinear DCmG system is transformed into Brunovsky's canonical form. Other approaches, such as those in [22]–[24], approximated nonlinear DCmGs with CPLs as linear systems, using polytopic set-based control techniques [22] or T-S fuzzy control methods [23], [24]. However, these methods typically assume that CPL dynamics need to satisfy the Lipschitz or bounded constraints, which are strong assumptions, limiting their applicability to the complex nonlinearities encountered in DCmGs. Moreover, their effectiveness is restricted by the specific DCmG sizes and topologies, making them non-scalable for frequent PnP operations of DGUs.

Scalable control methods are essential for ensuring seamless PnP operations of DGUs while maintaining voltage stability of DCmGs [18]. In recent years, several scalable control schemes have been extensively developed in DCmGs. For instance, Wang *et al.* [25] proposed a scalable reliable voltage control scheme using a structured free-weight matrix (SFWM) to mitigate the coupling effects of power lines. Eliminating the line coupling is critical for scalability of DCmGs, as the plugging-in/-out of DGUs alters the coupling configuration of power lines. In this regard, a scalable robust voltage control method adopting a structured slack matrix (SSM) was introduced in [26], and a scalable optimal voltage control approach was developed utilizing a structured Lyapunov matrix (SLM) [27]. Furthermore, a SLM-based scalable fault-tolerant control strategy was proposed in [28] against actuator faults. While these scalable control methods enable smooth PnP operations, they fail to address the nonlinearities and negative impedance effects associated with CPLs. Moreover, their controller designs require solving linear matrix inequality

TABLE I: Comparative Analysis Between the Contributions of This Paper and the Existing Results in the Literature

Refs.[1]	VSUCPL[2]	Sca.[3]	SANCPL[4]	WRLBCPL[5]	MES[6]
[19]	✓	✗	BC[7]	✗	–
[20]	✓	✗	JL[8]	✗	–
[21]	✓	✗	BM[9]	✗	–
[22]	✓	✗	PS[10]	✗	–
[23]	✓	✗	T-SFR[11]	✗	–
[24]	✓	✗	T-SFR	✗	–
[25]	✗	✓	–	–	SFWM[12]
[26]	✗	✓	–	–	SSM[13]
[27]	✗	✓	–	–	SLM[14]
[28]	✗	✓	–	–	SLM
†[15]	✓	✓	RBFNN[16]	✓	SLM

[1]References. [2]Voltage stabilization under CPL. [3]Scalability.
[4]Solutions for addressing the nonlinearity of CPL.
[5]Without requiring Lipschitz or boundedness of CPL.
[6]Methods for ensuring scalability. [7]Bounded condition.
[8]Jacobian linearization. [9]Backstepping method. [10]Polytopic set.
[11]T-S fuzzy rule. [12]Structured free-weight matrix.
[13]Structured slack matrix. [14]Structured Lyapunov matrix.
[15]This paper. [16]Radial basis function neural network.

(LMI) problems with structured matrices, often resulting in numerical infeasibility or over-conservatism.

Motivated by these observations, the following challenges will be addressed:

1) How to stabilize voltage in nonlinear DCmGs without the need for prior knowledge of CPLs?
2) How to design a control method that enables the seamless PnP operations of DGUs under CPLs?
3) How to ensure that the proposed controller design is numerically solvable, thus preventing rejection of plug-in/-out requests?

To cope with these challenges, this paper proposes a scalable neural network control scheme for voltage stabilization in DCmGs with CPLs. A comparative analysis of the existing results in the literature is provided in Table I. It highlights that existing results primarily focus on either voltage stabilization with prior CPL knowledge or scalability without CPLs. In contrast, the proposed control scheme employs a scalable neural network to enable PnP operations of DGUs with CPLs while eliminating the need for prior CPL knowledge. The main contributions of this paper are summarized as follows:

1) Unlike linear [19], [20], nonlinear [21], and approximated linear methods [22]–[24] that rely on Lipschitz or bounded conditions of CPLs, this paper employs a radial basis function (RBF) neural network to accurately approximate CPL nonlinearities without any prior knowledge, providing a flexible and practical solution for nonlinear DCmGs.
2) A scalable neural network control mechanism is proposed based on a structured Lyapunov matrix, ensuring uniformly ultimately bounded (UUB) stability even during plug-in/-out operations of DGUs with CPLs. By transforming the coupling effects of power lines into a Laplacian structure within the admittance matrix, this mechanism enables local operation, independent of both the number of DGUs and the coupling configuration of power lines, thus enhancing scalability.
3) Compared to traditional scalable control methods that are based on solving LMIs with structured matrices, e.g., SFWM [25], SSM [26], and SLM [27], [28], which often lead to numerical infeasibility and excessive conservatism, this paper develops explicit inequalities for nominal controller in conjunction with an adaptive controller. This design is inherently feasible, eliminating numerical infeasibility and ensuring that all plug-in/-out requests for DGUs are permitted.

Notations: Let $\mathbb{R}^{m\times n}$ denote the space of all real matrices of dimensions $m \times n$, and $\mathbf{0}^{m\times n}$ represent the null matrix of the same size. For any square matrix $G \in \mathbb{R}^{n\times n}$, the notation $G < 0$ (or $G > 0$) indicates that G is negative definite (or positive definite). The symbol $*$ is used to represent symmetric elements in a symmetric matrix. The operator $\mathrm{diag}\{z\}$, for a vector $z \in \mathbb{R}^n$, generates a diagonal matrix with the components of z as its diagonal entries. $\lambda_{\max}(H)$ and $\lambda_{\min}(H)$ denote the largest and smallest eigenvalues of a matrix H, respectively. $\mathbf{S}_n|\mathbb{S}^+_{n+1}$ indicates the plugging-in of a new subsystem $\mathbb{S}_{n+1}$ into system $\mathbf{S}_n$, while $\mathbf{S}_n|\mathbb{S}^-_{n-1}$ signifies the plugging-out of an existing subsystem $\mathbb{S}_{n-1}$ from $\mathbf{S}_n$.

This paper is structured as follows. Section II introduces the DCmG model and problem formulation. Section III presents the UUB stability analysis and scalable neural network controller design. Section IV outlines PnP operations. Section V provides simulation results. Section VI concludes this work.

II. System Modeling and Problem Formulation

Graph Theory: The system topology is represented by a connected graph $\mathcal{G} = (\mathcal{V}, \mathcal{E}, \mathcal{A})$, where $\mathcal{V} = 1, 2, \ldots, n$ denotes the set of nodes, $\mathcal{E} \subset \mathcal{V} \times \mathcal{V}$ represents the set of edges, and $\mathcal{A} = [a_{ij}] \in \mathbb{R}^{n\times n}$ is the adjacency matrix. For each node $i \in \mathcal{V}$, the condition $a_{ii} = 0$ ensures that there is no self-loop in the local information flow. If an edge $(j, i) \in \mathcal{E}$ exists, information flows from node j to i with an associated weight $a_{ij} > 0$; otherwise, $a_{ij} = 0$. The set of neighbors of node i is denoted by $\mathcal{N}_i$. The in-degree matrix is defined as $\mathcal{D} = \mathrm{diag}(\varkappa_i) \in \mathbb{R}^{n\times n}$, where $\varkappa_i = \sum_{j\in\mathbb{N}_i} a_{ij}$. The Laplacian matrix $\mathcal{L} = \mathcal{D} - \mathcal{A}$ is symmetric, positive semi-definite, and has non-negative off-diagonal elements.

TABLE II: Nomenclatures of the Local DCmG Parameters

Nomenclature	Electrical parameters
U_i	PCC voltage
$U_{\mathrm{ref}i}$	Reference voltage
U_{si}	Source voltage
$\mathcal{U}_i$	Integrator state
I_i	Filter current
R_{fi}	Resistance of the RLC filter
L_{fi}	Inductance of the RLC filter
C_{fi}	Capacitance of the RLC filter
R_{ij}	Resistance of the power line
L_{ij}	Inductance of the power line
$P_{\ell i}$	Power consumed by the CPL.
d_i	Duty cycle of the converter

As shown in Fig. 1, the interconnected DCmGs are depicted in a decentralized configuration, where power lines serve as the sole communication medium, modeled as RL circuits [27]. Each subsystem consists of a renewable DGU, a local controller, and a local CPL. The DGU consists of a buck converter,

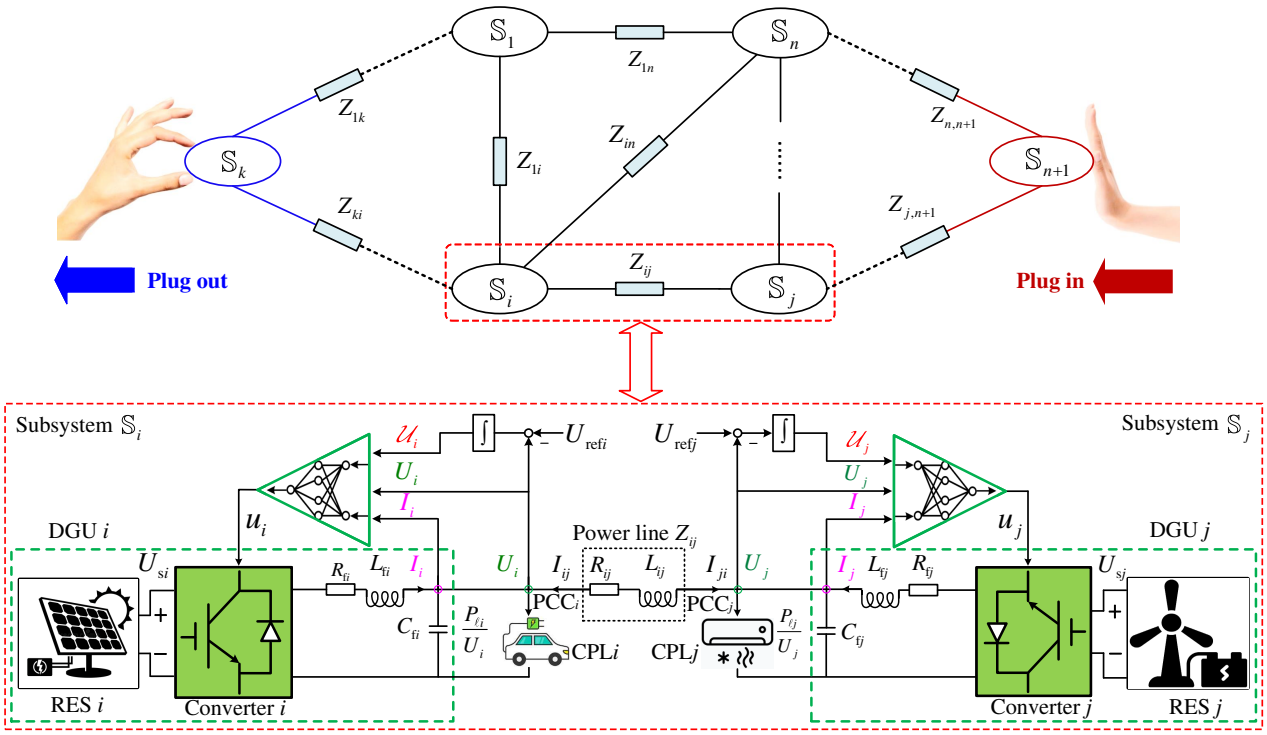

Fig. 1: Framework of scalable neural network control for nonlinear DCmGs under plugging-in/-out operations.

a series RLC filter, and a DC voltage source representing a RES. The buck converter interfaces between the DGU and the controller, which regulates the power supply to the load connected at the point of common coupling (PCC). Detailed descriptions of the local parameters are provided in Table II.

A. Local Model of a DGU With a CPL

By applying the Kirchhoff's voltage and current laws to the local DGU and power line depicted in Fig. 1, the following local system dynamics are obtained:

$$\dot{U}_i = \frac{1}{C_{\mathrm{f}i}} I_i + \frac{1}{C_{\mathrm{f}i}} I_{ij} - \frac{P_{\ell i}}{C_{\mathrm{f}i} U_i} \tag{1a}$$

$$\dot{I}_i = -\frac{R_{\mathrm{f}i}}{L_{\mathrm{f}i}} I_i - \frac{1}{L_{\mathrm{f}i}} U_i + \frac{d_i}{L_{\mathrm{f}i}} U_{si} \tag{1b}$$

$$\dot{I}_{ij} = \frac{1}{L_{ij}} U_j - \frac{1}{L_{ij}} U_i - \frac{R_{ij}}{L_{ij}} I_{ij}. \tag{1c}$$

Using the quasi-stationary-line (QSL) approximation [29] for power lines, i.e., $\dot{I}_{ij} = 0$, the line dynamics in (1c) can be simplified as

$$I_{ij} = \frac{1}{R_{ij}} \left(U_j - U_i \right). \tag{2}$$

According to IEEE standards [30], a key requirement for the local controller is to ensure voltage stability in DCmGs by accurately tracking the reference voltage $U_{\mathrm{ref}i}$, thereby minimizing voltage deviations. To eliminate static error, the following integrator is introduced:

$$\dot{\mathcal{U}}_i = U_{\mathrm{ref}i} - U_i \tag{3}$$

where $U_{\mathrm{ref}i}$ is treated as a constant because it represents the target operating voltage for each DGU, set based on standard conditions for stable and efficient power distribution. The integrator state $\mathcal{U}_i$ represents the accumulated voltage error at the PCC$_i$.

Therefore, the dynamics of the local DCmG model are described as follows:

$$\begin{cases} \dot{U}_i = \dfrac{1}{C_{\mathrm{f}i}} I_i + \displaystyle\sum_{j \in \mathcal{N}_i} \frac{U_j - U_i}{C_{\mathrm{f}i} R_{ij}} - \frac{P_{\ell i}}{C_{\mathrm{f}i} U_i} \\ \dot{I}_i = -\dfrac{R_{\mathrm{f}i}}{L_{\mathrm{f}i}} I_i - \dfrac{1}{L_{\mathrm{f}i}} U_i + \dfrac{d_i}{L_{\mathrm{f}i}} U_{si} \\ \dot{\mathcal{U}}_i = U_{\mathrm{ref}i} - U_i. \end{cases} \tag{4}$$

For an equilibrium point $[U_{0i}, U_{0j}, I_{0i}, \mathcal{U}_{0i}, d_{0i}]$, the following condition holds:

$$P_{\ell i} < \min \left\{ \frac{U_{si}}{4R_{\mathrm{f}i}}, \frac{R_{\mathrm{f}i} C_{\mathrm{f}i} U_{0i}^2}{L_{\mathrm{f}i}} \right\} = P_{\ell i}^{\max}$$

where $P_{\ell i}^{\max}$ denotes the maximum power demand of the lcoal CPL by linearizing the system (4) around the equilibrium point [24]. After implementing a change of coordinates at the equilibrium point, the system can be rewritten as

$$\begin{cases} \dot{\overline{U}}_i = \dfrac{1}{C_{\mathrm{f}i}} \overline{I}_i + \displaystyle\sum_{j \in \mathcal{N}_i} \frac{\overline{U}_j - \overline{U}_i}{C_{\mathrm{f}i} R_{ij}} - \frac{1}{C_{\mathrm{f}i}} f_i(\overline{U}_i) \\ \dot{\overline{I}}_i = -\dfrac{R_{\mathrm{f}i}}{L_{\mathrm{f}i}} \overline{I}_i - \dfrac{1}{L_{\mathrm{f}i}} \overline{U}_i + \dfrac{\overline{d}_i}{L_{\mathrm{f}i}} U_{si} \\ \dot{\overline{\mathcal{U}}}_i = -\overline{U}_i \end{cases} \tag{5}$$

where

$$\overline{U}_i = U_i - U_{0i}, \overline{U}_j = U_j - U_{0j}, \overline{\mathcal{U}}_i = \mathcal{U}_i - \mathcal{U}_{0i},$$

$$\overline{I}_i = I_i - I_{0i}, \overline{d}_i = d_i - d_{0i}, f_i(\overline{U}_i) = \frac{P_{\ell i} \overline{U}_i}{U_{0i}(\overline{U}_i + U_{0i})}.$$

The state-space model of (5) is expressed as

$$\begin{aligned}\mathbb{S}_i : \dot{x}_i(t) &= A_{ii}x_i(t) + B_i u_i(t) + D_i f_i(x_i(t)) \\ &+ \sum\nolimits_{j\in\mathcal{N}_i} A_{ij}\big(x_j(t) - x_i(t)\big)\end{aligned} \tag{6}$$

where $x_i = [\overline{U}_i, \overline{I}_i, \overline{\mathcal{U}}_i]^T$ represents the state vector of $\mathbb{S}_i$, and x_j denotes the state vector of $\mathbb{S}_j$, for $i \in \mathcal{V}$, $j \in \mathcal{N}_i$. The control input is denoted by $u_i = \overline{d}_i U_{si}$. The function $f_i(x_i(t))$ represents the unknown nonlinearity of the CPL. The term $\sum_{j\in\mathcal{N}_i} A_{ij}(x_j(t) - x_i(t))$ denotes the coupling of power lines, with A_{ij} being the corresponding coupling matrix. The relevant matrices are given as

$$A_{ii} = \begin{bmatrix} 0 & \frac{1}{C_{fi}} & 0 \\ -\frac{1}{L_{fi}} & -\frac{R_{fi}}{L_{fi}} & 0 \\ -1 & 0 & 0 \end{bmatrix},\ B_i = \begin{bmatrix} 0 \\ \frac{1}{L_{fi}} \\ 0 \end{bmatrix},$$

$$A_{ij} = \begin{bmatrix} \frac{1}{C_{fi}R_{ij}} & 0 & 0 \\ 0 & 0 & 0 \\ 0 & 0 & 0 \end{bmatrix},\ D_i = \begin{bmatrix} \frac{1}{C_{fi}} \\ 0 \\ 0 \end{bmatrix}.$$

Remark 1: The local DCmG system (6) is an approximate model based on the following assumptions: 1) The RES is modeled as an ideal DC voltage source, justified by the slow timescale of typical RES power generation fluctuations and the inclusion of energy storage units that stabilize stochastic variations in power output [26]. 2) The switching dynamics of the buck converter are simplified using standard space averaging techniques [27], allowing the converter output to be approximated as $u_i = \overline{d}_i U_{si}$, where U_{si} is sufficiently large to avoid saturation of $\overline{d}_i \in [0, 1]$. 3) The QSL approximation for line dynamics is adopted to model neutral interactions among DGUs, as expressed in (2), with its validity supported by singular perturbation theory [29]. 4) CPLs are connected at the PCC through an RLC filter, enabling interconnections to be represented using the Kron reduction method [31].

B. Global DCmG Model With n DGUs With CPLs

The global DCmG system, comprising n DGUs with CPLs, can be described as follows:

$$\mathbf{S}_n :\ \dot{\boldsymbol{x}}(t) = \boldsymbol{A}\boldsymbol{x}(t) + \boldsymbol{B}\boldsymbol{u}(t) + \boldsymbol{D}\boldsymbol{f}(\boldsymbol{x}(t)) \tag{7}$$

where

$$\begin{aligned}\boldsymbol{x}(t) &= \left[x_1^T(t), x_2^T(t), \ldots, x_n^T(t)\right]^T, \\ \boldsymbol{u}(t) &= \left[u_1^T(t), u_2^T(t), \ldots, u_n^T(t)\right]^T, \\ \boldsymbol{f}(t) &= \left[f_1^T(x_1(t)), f_2^T(x_2(t)), \ldots, f_n^T(x_n(t))\right]^T,\end{aligned}$$

and

$$\boldsymbol{A} = \begin{bmatrix} A_{11} + A_{d1} & A_{12} & \cdots & A_{1n} \\ A_{21} & A_{22} + A_{d2} & \cdots & A_{2n} \\ \vdots & \vdots & \ddots & \vdots \\ A_{n1} & A_{n2} & \cdots & A_{nn} + A_{dn} \end{bmatrix},$$

$$\boldsymbol{B} = \operatorname{diag}\{B_1, B_2, \ldots, B_n\},\ \boldsymbol{E} = \operatorname{diag}\{E_1, E_2, \ldots, E_n\}.$$

In (7), the global system matrix $\boldsymbol{A}$ is decomposed into three distinct parts as follows:

$$\boldsymbol{A} = \boldsymbol{A}_v + \boldsymbol{A}_d + \boldsymbol{A}_a \tag{8}$$

where $\boldsymbol{A}_v = \operatorname{diag}\{A_{11}, A_{22}, \ldots, A_{nn}\}$ collects the dynamic behavior of all DGUs. The terms $\boldsymbol{A}_d$ and $\boldsymbol{A}_a$ denote the coupling effects of power lines. Specifically, $\boldsymbol{A}_d = \operatorname{diag}\{A_{d1}, A_{d2}, \ldots, A_{dn}\}$, where each block is given as

$$A_{di} = \begin{bmatrix} -\sum\limits_{j\in\mathcal{N}_i} \frac{1}{R_{ij}C_{fi}} & \mathbf{0}^{1\times 2} \\ \mathbf{0}^{2\times 1} & \mathbf{0}^{2\times 2} \end{bmatrix} \tag{9}$$

reflecting the dependence of each local state on neighboring DGUs. Additionally, $\boldsymbol{A}_a$ captures the interaction effects across power lines, consisting of zero diagonal blocks and off-diagonal blocks A_{ij}.

C. Description of RBF Neural Network

In a DCmG system, CPLs exhibit nonlinear characteristics that correspond to first-third quadrant hyperbolas in the voltage-current relationship. These nonlinearities are intrinsically dynamic and dependent on functional conditions [13]. As these loads are not explicitly know a priori, their nonlinear behaviors pose significant challenges for direct modeling and control, introducing considerable uncertainty into the system. Because of the unknown and variable nature of these nonlinearities, traditional linear modeling approaches are often inadequate, thereby necessitating the use of advanced approximation methods, such as neural networks.

RBF neural networks are well-established for their capacity to approximate unknown smooth nonlinear functions [32]. Within the context of DCmGs, RBF neural networks are particularly suited for capturing the continuous nonlinear dynamics associated with CPLs. Thus, they can be utilized to approximate the unknown nonlinear function $f_i(x_i(t))$ in (6).

An RBF neural network $f_{\text{RBF}}(X)$ approximates any continuous function $f(X) : \mathbb{R}^n \to \mathbb{R}$ and is expressed as

$$f_{\text{RBF}}(X) = \Psi^T \psi(X) \tag{10}$$

where $X \in \Phi \subset \mathbb{R}^q$ is the input vector, with q representing the input dimension of the neural network. $\Psi = [\phi_1, \phi_2, \ldots, \phi_l]^T \in \mathbb{R}^l$ denotes the weight vector, where l is the number of neurons. The basis function vector $\psi(X) = [\varrho_1(X), \varrho_2(X), \ldots, \varrho_l(X)]^T$ consists of the following Gaussian functions:

$$\varrho_i(X) = \exp\left[-\frac{(X - \vartheta_i)^T(X - \vartheta_i)}{\delta_i^2}\right] \tag{11}$$

where δ_i is the width of the Gaussian function, and $\vartheta_i = [\vartheta_{i1}, \vartheta_{i2}, \ldots, \vartheta_{iq}]$ represents the center of the receptive field.

As shown in [32], when the number of nodes l is sufficiently large, the RBF network (10) can approximate any continuous function $f(X)$ over a compact set $\Phi \subset \mathbb{R}^q$ with arbitrary accuracy $\overline{\varphi} > 0$. This approximation is represented as

$$f(X) = \Psi^{*T}\psi(X) + \varphi(X) \tag{12}$$

where $\Psi^* = \arg\min_{\psi\in\mathbb{R}^l}\{\sup_{X\in\Phi}|f(X) - \Psi^T\psi(X)|\}$ represents the ideal weight vector minimizing the supremum of the approximation error over Φ, and $\varphi(X)$ is the approximation error, satisfying $\varphi(X) \le \overline{\varphi}$.

Remark 2: The approximation accuracy of RBF neural networks directly affects the control performance in DCmGs.

A more accurate model, achieved by increasing the number of neurons, reduces the approximation error $\varphi(X)$ and enhances control precision. However, this improvement increases computational complexity, potentially hindering real-time implementation. Alternative neural networks, such as deep neural networks (DNNs) or convolutional neural networks (CNNs), can achieve higher fidelity in approximating nonlinearities but often require extensive training datasets and significant computational resources, making them less practical for real-time control. The RBF neural network is employed in this work for its efficiency in approximating smooth nonlinearities associated with CPLs while balancing accuracy, computational cost, and real-time applicability.

D. Local Controller Design

The RBF neural networks are employed alongside an adaptive control method to facilitate online parameter approximation and estimation. $\widehat{\xi}_{iq}(t)$ $(i \in \mathcal{V}, q = 1, 2, \ldots, r)$ is the online estimate of $\xi_{iq} = \|\Psi_i\|^2$, where $\xi_i = [\xi_{i1}, \xi_{i2}, \ldots, \xi_{ir}]^T$.

According to [25], the pair (A_{ii}, B_i) is controllable. Therefore, the local neural network controller for subsystem $\mathbb{S}_i$ (6) are designed as follows:

$$\mathbb{C}_i : u_i(t) = K_i x_i(t) + \widehat{u}_i(t) \tag{13}$$

where $K_i = [k_{1i}\ k_{2i}\ k_{3i}] \in \mathbb{R}^{1\times 3}$ represents the nominal controller gain, and the adaptive controller $\widehat{u}_i(t)$ is formulated as follows:

$$\widehat{u}_i(t) = -\frac{\widehat{\xi}_i(t)}{2\delta_i^2}\psi_i^T(x_i(t))\psi_i(x_i(t))\left\|B_i\right\|^{-1}\left\|P_i D_i\right\| D_i^T x_i(t) \tag{14}$$

with the adaptation law defined as

$$\dot{\widehat{\xi}}_{iq}(t) = \frac{\zeta_{iq}}{2\delta_{iq}^2}\psi_i^T(x_i(t))\psi_i(x_i(t))\|P_i D_i\|^2 x_i^2(t) \tag{15}$$

where ζ_{iq} $(q = 1, ..., r)$ represents the adaptive gain. The term $\psi_i(x_i(t))$ denotes the basis function vector, and P_i is the Lyapunov matrix, which will be discussed in the sequal.

Remark 3: The decentralized control framework presented in this paper is specifically designed for DCmGs with physical power line connections, eliminating the need for communication networks among subsystems. This architecture brings several key advantages [10], [33]:

1) Scalability: This framework facilitates the seamless connection or disconnection of DGUs, making it well-suited for applications requiring flexible and scalable system architecture.

2) Simplicity: By avoiding complex communication setups, the system simplifies the deployment and management, which is advantageous in practical applications with limited computational resources.

3) Resilience: The independent functionality of each subsystem enhances resilience against communication delays, cyber threats, and privacy issues.

4) Redundancy: The decentralized control approach builds redundancy by distributing control tasks across subsystems, minimizing reliance on any single unit and ensuring continued functioning despite individual failures.

III. UUB Stability Analysis and Scalable Neural Network Controller Design

In this section, the UUB stability criteria is presented for the DCmG system described by (6), excluding the coupling term $\sum_{j\in\mathcal{N}_i} A_{ij}(x_j(t) - x_i(t))$. Specifically, the focus is on the dynamics: $\dot{x}_i(t) = A_{ii}x_i(t) + B_i u_i(t) + D_i f_i\big(x_i(t)\big)$. The primary result is summarized in the following theorem.

Theorem 1: For $i \in \mathcal{V}$, the closed-loop local DCmG system $\mathbb{S}_i$, excluding the coupling term $\sum_{j\in\mathcal{N}_i} A_{ij}(x_j(t) - x_i(t))$, is UUB if there exists an arbitrary positive definite matrix P_i and a nominal controller gain matrix K_i belonging to the set:

$$\mathcal{K}_i = \left\{ \begin{array}{c} k_{1i} < 1, \\ k_{2i} < R_{\mathrm{fi}}, \\ 0 < k_{3i} < \dfrac{1}{L_{\mathrm{fi}}}(k_{1i} - 1)(k_{2i} - R_{\mathrm{fi}}) \end{array} \right\} \tag{16}$$

such that the following condition holds:

$$Q_i = P_i A_{ii} + A_{ii}^T P_i + P_i B_i K_i + K_i^T B_i^T P_i < 0 \tag{17}$$

under the adaptive controller $\widehat{u}_i(t)$ defined in (14) with the adaptation law given by (15).

Proof: Define the adaptive error variable as

$$\widetilde{\xi}_{iq}(t) = \widehat{\xi}_{iq}(t) - \xi_{iq} \tag{18}$$

and consider the following Lyapunov function:

$$V_i(t) = V_{1i}(t) + V_{2i}(t) \tag{19}$$

where $V_{1i}(t) = x_i^T(t)P_i x_i(t)$ and $V_{2i}(t) = \sum_{q=1}^{r} \frac{\widetilde{\xi}_{iq}^2(t)}{\zeta_{iq}}$.

The time derivative of $V_{1i}(t)$ along the trajectories of $\mathbb{S}_i$ is given by

$$\begin{aligned} \dot{V}_{1i}(t) &= x_i^T(t)Q_i x_i(t) + 2x_i^T(t)P_i B_i \widehat{u}_i(t) \\ &\quad + 2x_i^T(t)P_i D_i f_i(x_i(t)) \\ &= x_i^T(t)Q_i x_i(t) + 2x_i^T(t)P_i D_i f_i(x_i(t)) \\ &\quad - x_i^T(t)\frac{\widehat{\xi}_i(t)}{\delta_i^2}\psi_i^T(x_i(t))\psi_i(x_i(t))\|P_i D_i\|^2 x_i(t). \end{aligned} \tag{20}$$

Similarly, the time derivative of $V_{2i}(t)$ is

$$\begin{aligned} \dot{V}_{2i}(t) &= 2\sum_{q=1}^{r}\frac{\widetilde{\xi}_{iq}(t)\dot{\widetilde{\xi}}_{iq}(t)}{\zeta_{iq}} \\ &= \sum_{q=1}^{r}\frac{\widetilde{\xi}_{iq}(t)}{\delta_{iq}^2}\psi_i^T(x_i(t))\psi_i(x_i(t))\|P_i D_i\|^2 x_i^2(t). \end{aligned} \tag{21}$$

For the unknown nonlinearity $f_i(x_i(t))$ of the CPL in (20), one has

$$\begin{aligned} &2x_i^T(t)P_i D_i f_i(x_i(t)) = -\|P_i D_i\|^2 x_i^2(t) \\ &\quad + 2x_i^T(t)P_i D_i\big[f_i(x_i(t)) + 0.5\|P_i D_i\|x_i^2(t)\big] \\ &\leq 2x_i^T(t)P_i D_i F_i(x_i(t)) - \|P_i D_i\|^2 x_i^2(t) \end{aligned} \tag{22}$$

where $F_i(x_i(t)) = f_i(x_i(t)) + 0.5\|P_i D_i\|x_i^2(t)$. Since $F_i(x_i(t))$ is unknown and cannot be directly implemented, it is approximated using the RBF neural network $\Psi_i^T\psi_i(x_i(t))$, leading to

$$F_i(x_i(t)) = \Psi_i^T\psi_i(x_i(t)) + \varphi_i(x_i(t)), \varphi_i(x_i(t)) \leq \overline{\varphi}_i. \tag{23}$$

Substituting (23) into (22) and applying the basic inequality $2ab \leq a^2 + b^2$, it can be obtained that

$$\begin{aligned}
&2x_i^T(t)P_iD_if_i(x_i(t)) \leq 2x_i^T(t)P_iD_i\Psi_i^T\psi_i(x_i(t)) \\
&+ 2x_i^T(t)P_iD_i\varphi_i(x_i(t)) - \|P_iD_i\|^2 x_i^2(t) \\
&\leq \sum_{q=1}^{r}\left(\frac{\xi_{iq}}{\delta_{iq}^2}\psi_i^T(x_i(t))\psi_i(x_i(t))\|P_iD_i\|^2 x_i^2(t) + \delta_{iq}^2\right) \\
&+ \|P_iD_i\|^2 x_i^2(t) + \overline{\varphi}_i^2 - \|P_iD_i\|^2 x_i^2(t) \\
&\leq \sum_{q=1}^{r}\left(\frac{\xi_{iq}}{\delta_{iq}^2}\psi_i^T(x_i(t))\psi_i(x_i(t))\|P_iD_i\|^2 x_i^2(t) + \delta_{iq}^2\right) + \overline{\varphi}_i^2
\end{aligned} \tag{24}$$

where $\xi_{iq} = \|\Psi_i\|^2$ is an unknown parameter. $\left(x_i^T(t)P_iD_i\Psi_i^T\psi_i(x_i(t))\right)_q$ denotes the q-th element of $x_i^T(t)P_iD_i\Psi_i^T\psi_i(x_i(t))$.

Combining (18), (20), (21), and (24) yields

$$\begin{aligned}
\dot{V}_i(t) &= \dot{V}_{1i}(t) + \dot{V}_{2i}(t) \\
&= x_i^T(t)Q_ix_i(t) + \sum_{q=1}^{r}\delta_{iq}^2 + \overline{\varphi}_i^2 \\
&\quad - x_i^T(t)\frac{\widehat{\xi}_i(t)}{\delta_i^2}\psi_i^T(x_i(t))\psi_i(x_i(t))\|P_iD_i\|^2 x_i(t) \\
&\quad + \sum_{q=1}^{r}\frac{\widetilde{\xi}_{iq}(t)}{\delta_{iq}^2}\psi_i^T(x_i(t))\psi_i(x_i(t))\|P_iD_i\|^2 x_i^2(t) \\
&\quad + \sum_{q=1}^{r}\left(\frac{\xi_{iq}}{\delta_{iq}^2}\psi_i^T(x_i(t))\psi_i(x_i(t))\|P_iD_i\|^2 x_i^2(t)\right) \\
&\leq x_i^T(t)Q_ix_i(t) + \sum_{q=1}^{r}\delta_{iq}^2 + \overline{\varphi}_i^2.
\end{aligned} \tag{25}$$

Considering $\dot{V}_i(t) \leq x_i^T(t)Q_ix_i(t) + \sum_{q=1}^{r}\delta_{iq}^2 + \overline{\varphi}_i^2$, it can be concluded that $\dot{V}_i(t) < 0$ if the following condition is satisfied:

$$\|x_i(t)\| > \alpha_i \tag{26}$$

where $\alpha_i = \left[\left(\sum_{q=1}^{r}\delta_{iq}^2 + \overline{\varphi}_i^2\right)/(-\lambda_{\max}(Q_i))\right]^{(1/2)}$.

Thus, $\dot{V}_i(t)$ is negative definite outside the compact set $\Omega_{\alpha_i} =: \{x_i | \|x_i(t)\| \leq \alpha_i\}$, meaning that whenever $\|x_i(t)\|$ exits this set, $V_i(t)$ will decrease, and $\|x_i(t)\|$ will remain bounded with the ultimate bound α_i.

Furthermore, since $Q_i < 0$ in (17), it can be deduced that there exists a positive scalar β_i such that

$$\dot{V}_i(t) \leq -\beta_i V_i(t) + \sum_{q=1}^{r}\delta_{iq}^2 + \overline{\varphi}_i^2. \tag{27}$$

Multiplying both sides of (27) by $e^{\beta_i t}$ and integrating, one obtains

$$V_i(t) \leq V_i(0) + \left(\sum_{q=1}^{r}\delta_{iq}^2 + \overline{\varphi}_i^2\right)\beta_i^{-1}.$$

According to the similar method in [34], one has

$$x_i^T(t)P_ix_i(t) \leq V_i(t) \leq V_i(0) + \left(\sum_{q=1}^{r}\delta_{iq}^2 + \overline{\varphi}_i^2\right)\beta_i^{-1}.$$

Therefore, it can be obtained that

$$\|x_i(t)\| \leq \gamma_i \tag{28}$$

where $\gamma_i = \left[\left(V_i(0) + \left(\sum_{q=1}^{r}\delta_{iq}^2 + \overline{\varphi}_i^2\right)\beta_i^{-1}\right)/\lambda_{\min}(P_i)\right]^{(1/2)}$.

From (26) and (28), one can conclude that

$$\alpha_i < \|x_i(t)\| \leq \gamma_i. \tag{29}$$

Based on the above analyses, it has been shown that all solutions of DCmGs will start in a ball $\Omega_{\gamma_i} =: \{x_i \,|\alpha_i < \|x_i(t)\| \leq \gamma_i\}$, enter the smaller ball Ω_{α_i}, and ultimately be bounded by a scalar α_i, which is consistent with definition 4.6 in [35]. Thus, the proof of UUB stability is completed.

Remark 4: Theorem 1 addresses the challenge of the unknown nonlinearity $f_i(x_i(t)$ introduced by CPLs, with the RBF neural network $\Psi_i^T\psi_i(x_i(t))$ handling the nonlinearity without requiring prior knowledge. Existing approaches, such as the robust control strategy developed in [19], encounter challenges in dealing with unknown and unbounded CPLs. Jacobian linearization [20] struggles to balance improvements in settling time and overshoot performance [36]. Nonlinear backstepping control [21] may not fully address CPL nonlinearities in the presence of noise [37]. Additionally, linear approximations, as shown in [22]–[24], often lead to degraded performance due to their reliance on the Lipschitz conditions of CPLs, limiting their effectiveness.

Remark 5: The UUB stability analysis presented in Theorem 1 assumes the absence of line coupling $\sum_{j\in\mathcal{N}_i}A_{ij}(x_j(t) - x_i(t))$. When the coupling term is present, the stability condition in (17) may no longer be sufficient, particularly during the plug-in/-out operations, where coupling characteristics can vary. However, if the adverse effects of these line couplings can be mitigated, UUB stability can still be ensured by satisfying the local condition in (17), thereby demonstrating the scalability of the proposed approach.

To address the negative effects of line couplings on the stability condition, the following theorem provides a solution.

Theorem 2: The closed-loop global DCmGs $\mathbf{S}_n$, which consists of n DGUs interconnected through power lines, remains UUB during frequent PnP operations of DGUs under CPLs if there exists a positive definite matrix $\boldsymbol{P} = \text{diag}\{P_1, P_2, \ldots, P_n\}$, where each P_i is designed as the following fixed structure:

$$P_i = \begin{bmatrix} \overline{p}C_{\text{fi}} & \mathbf{0}^{1\times 2} \\ \mathbf{0}^{2\times 1} & \mathcal{P}_i \end{bmatrix}, \ \mathcal{P}_i > 0, \ \overline{p} > 0, \tag{30}$$

and a matrix $\boldsymbol{K} = \text{diag}\{K_1, K_2, \ldots, K_n\}$, where each nominal controller gain matrix K_i belongs to the set $\mathcal{K}_i$ as described in (16), such that the following condition holds:

$$\boldsymbol{A}^T\boldsymbol{P} + \boldsymbol{P}\boldsymbol{A} + \boldsymbol{K}^T\boldsymbol{B}^T\boldsymbol{P} + \boldsymbol{P}\boldsymbol{B}\boldsymbol{K} < 0. \tag{31}$$

under the local adaptive controller defined in $\widehat{u}_i(t)$ (14) with the adaptation law given by (15).

Proof: Based on the decomposition of $\boldsymbol{A}$ given in (8), the term $\boldsymbol{A}^T\boldsymbol{P}+\boldsymbol{P}\boldsymbol{A}$ in (31) can be expanded as follows:

$$\boldsymbol{A}^T\boldsymbol{P}+\boldsymbol{P}\boldsymbol{A}=\boldsymbol{A}_v^T\boldsymbol{P}+\boldsymbol{P}\boldsymbol{A}_v + \left(\overbrace{\underbrace{\boldsymbol{A}_d^T\boldsymbol{P}+\boldsymbol{P}\boldsymbol{A}_d}_{\text{(a)}}+\underbrace{(\boldsymbol{A}_a^T\boldsymbol{P}+\boldsymbol{P}\boldsymbol{A}_a)}_{\text{(b)}}}^{\text{(c)}}\right) \tag{32}$$

where term *(a)* is a block diagonal matrix representing the dependence of the global system state on neighboring DGUs, with each block given by $A_{di}^TP_i+P_iA_{di}$. Term *(b)* denotes the coupling effects of power lines, consisting of blocks with zeros on the diagonal and off-diagonal blocks of $A_{ji}^TP_j+P_iA_{ij}$, for $i\in\mathcal{V},\ j\in\mathcal{N}_i$. Additionally, term *(c)* captures the destabilizing effects due to line couplings.

For term *(a),* recalling the matrix A_{di} given in (9) and the structured Lyapunov matrix P_i defined in (30), it can be obtained that it's each block is given by

$$A_{di}^TP_i+P_iA_{di}=\begin{bmatrix}-\sum\limits_{j\in\mathcal{N}_i}\frac{2\overline{p}}{R_{ij}} & \mathbf{0}^{1\times2}\\ \mathbf{0}^{2\times1} & \mathbf{0}^{2\times2}\end{bmatrix}\in\mathbb{R}^{3\times3}. \tag{33}$$

It is evident that the matrix in (33) has non-zero elements only in the (1, 1) position, with all other elements being zero. After removing the zero terms, define

$$\mathcal{D}_{ii}=-\sum_{j\in\mathcal{N}_i}\frac{2\overline{p}}{R_{ij}}$$

and by collecting these blocks, one obtains

$$\widehat{\mathcal{D}}=\operatorname{diag}\left\{\mathcal{D}_{11},\mathcal{D}_{22},\ldots,\mathcal{D}_{nn}\right\}. \tag{34}$$

For term *(b),* it can be rewritten as follows:

$$\begin{cases}A_{ji}^TP_j+P_iA_{ij}, & \text{if } i\in\mathcal{V}, j\in\mathcal{N}_i\\ 0, & \text{otherwise.}\end{cases}$$

Reminding the matrix A_{ij} presented in (6) and P_i (30), one has

$$A_{ji}^TP_j+P_iA_{ij}=\begin{bmatrix}\frac{2\overline{p}}{R_{ij}} & \mathbf{0}^{1\times2}\\ \mathbf{0}^{2\times1} & \mathbf{0}^{2\times2}\end{bmatrix}\in\mathbb{R}^{3\times3}. \tag{35}$$

Similarly, only the (1, 1) element is nonzero. Define $\mathcal{A}_{ij}$ as the non-zero entry, i.e.,

$$\mathcal{A}_{ij}=\begin{cases}\dfrac{2\overline{p}}{R_{ij}}, & \text{if } i\in\mathcal{V}, j\in\mathcal{N}_i\\ 0, & \text{otherwise.}\end{cases}$$

Collecting these blocks into the matrix

$$\widehat{\mathcal{A}}=\begin{bmatrix}0 & \mathcal{A}_{12} & \cdots & \mathcal{A}_{1n}\\ \mathcal{A}_{21} & 0 & \cdots & \mathcal{A}_{2n}\\ \vdots & \vdots & \ddots & \vdots\\ \mathcal{A}_{n1} & \mathcal{A}_{n2} & \cdots & 0\end{bmatrix}. \tag{36}$$

For term *(c),* define $\widehat{\mathcal{L}}=\widehat{\mathcal{D}}+\widehat{\mathcal{A}}$, yielding

$$\widehat{\mathcal{L}}=\begin{bmatrix}\mathcal{D}_{11} & \mathcal{A}_{12} & \cdots & \mathcal{A}_{1n}\\ \mathcal{A}_{21} & \mathcal{D}_{22} & \cdots & \mathcal{A}_{2n}\\ \vdots & \vdots & \ddots & \vdots\\ \mathcal{A}_{n1} & \mathcal{A}_{n2} & \cdots & \mathcal{D}_{nn}\end{bmatrix}. \tag{37}$$

By observing the structure of $\widehat{\mathcal{D}}$, it can be seen that $-\widehat{\mathcal{D}}$ corresponds to the in-degree matrix in graph theory, while $\widehat{\mathcal{A}}$ represents the adjacency matrix. Therefore, $-\widehat{\mathcal{L}}$ resembles the Laplacian matrix, implying symmetry and positive semidefiniteness. This means that

$$\widehat{\mathcal{L}}\leq0 \tag{38}$$

which implies that term *(c)* is non-positive, i.e.,

$$\boldsymbol{A}_d^T\boldsymbol{P}+\boldsymbol{P}\boldsymbol{A}_d+\boldsymbol{A}_a^T\boldsymbol{P}+\boldsymbol{P}\boldsymbol{A}_a\leq0. \tag{39}$$

Finally, recalling the local condition (17) from Theorem 1, one obtains

$$\boldsymbol{A}_v^T\boldsymbol{P}+\boldsymbol{P}\boldsymbol{A}_v+\boldsymbol{K}^T\boldsymbol{B}^T\boldsymbol{P}+\boldsymbol{P}\boldsymbol{B}\boldsymbol{K}<0. \tag{40}$$

Using the decomposition $\boldsymbol{A}=\boldsymbol{A}_v+\boldsymbol{A}_d+\boldsymbol{A}_a$ in (8), we derive the LMI condition (31) ultilizing the structured Lyapunov matrix (30). Thus, the proof is completed.

Remark 6: Theorem 2 provides a sufficient condition for achieving UUB stability in the global DCmG system $\mathbf{S}_n$, comprising n DGUs interconnected by power lines. By utilizing the structured Lyapunov matrix (30), the coupling effects among DGUs due to power line interconnections are transformed into a Laplacian structure, thereby eliminating these effects from the stability condition. This transformation enables the global UUB stability condition (31) to be interpreted as a straightforward aggregation of the local stability condition (17), independent of line couplings.

Remark 7: The structured Lyapunov matrix used in this paper adopts a block diagonal structure similar to those in [27], [28]. Unlike them, where the control design depends on LMI optimization and may yield a single control gain that is challenging to compute, the proposed method establishes the adaptive controller (14) governed by the adaptation law (15) and designs explicit inequalities for nominal controller (16), which are always solvable. Consequently, requests to plug-in/-out DGUs are never denied, ensuring the scalability for seamless PnP operations. Additionally, this scalability preserves the privacy of individual DGUs, as it does not require the disclosure of DGU model specifics or operational settings during PnP process, which is an essential feature in decentralized energy markets.

IV. PnP Operations

This section details the PnP operations of subsystems (DGUs and CPLs) in a DCmG while ensuring voltage stability.

1) Plugging-in operation: Consider a global DCmG $\mathbf{S}_n$ composed of n subsystems, each governed by the proposed scalable neural network control scheme $\mathbb{C}_i$ as defined in (13). When an additional subsystem $\mathbb{S}_{n+1}$ is plugged into $\mathbf{S}_n$, forming a new system $\mathbf{S}_{n+1}=\mathbf{S}_n|\mathbb{S}_{n+1}^+$, stability is preserved, provided that the controller $\mathbb{C}_{n+1}$ complies with the conditions specified in Theorem 2.

2) Plugging-out operation: The process of removing a subsystem is straightforward and does not disrupt the stability of the remaining subsystems. In an interconnected DCmG $\mathbf{S}_n$, where each subsystem is managed by the proposed controller $\mathbb{C}_i$, any DGU with CPL can be disconnected at any moment.

The resulting configuration, denoted as $\mathbf{S}_{n-1} = \mathbf{S}_n|\mathbb{S}_{n-1}^-$, remains stable because the local controller $\mathbb{C}_{n-1}$ requires only the individual subsystem's model.

V. Simulation Results

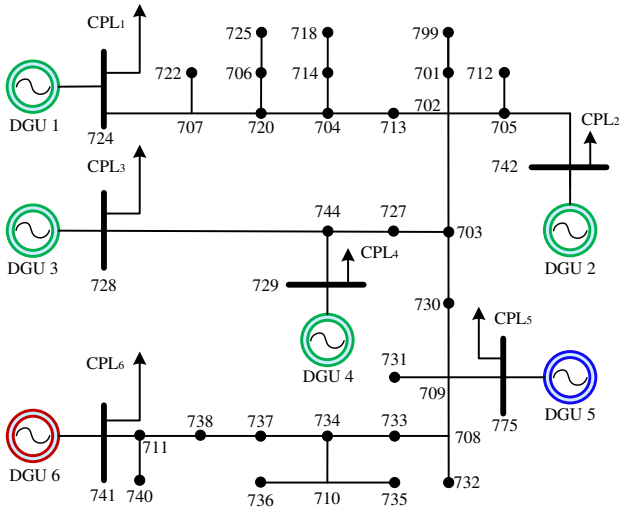

Fig. 2: The modified IEEE 37-bus test feeder.

TABLE III: Electrical Parameters for DCmG System

$\mathbb{S}_i$	$R_{\mathrm{f}}(\Omega)$	L_{f}(mH)	C_{f}(mF)	U_{ref}(V)	P_ℓ(W)
1	0.2	1.8	2.2	47	380
2	0.3	2.0	1.9	48	350
3	0.1	2.2	1.7	45	400
4	0.5	3.0	2.5	50	360
5	0.4	1.2	2.0	46	370
6	0.6	2.5	3.0	49	390

This section presents case studies conducted on a modified IEEE 37-bus test system [38], illustrated in Fig. 2. To demonstrate the effectiveness of the proposed control strategy, simulations are performed on the test system, which features six DGUs, with source voltages set to $U_{si} = 80$V and voltage reference values $U_{\mathrm{ref}i}$ (V) slightly varied to induce current flow I_{ij} through power lines in the asymptotic regime. The controller gains k_{1i}, k_{2i}, and k_{3i} are selected from the set $\mathcal{K}_i$ defined in (16). The value of $\bar{p} = 10$ is set for all DGUs. Additionally, the RBF neural network $\Psi_i^T\psi_i(x_i(t))$ comprises 11 nodes with centers evenly distributed in $[-5, 5] \times [-5, 5]$ and a width of two. The electrical parameters are provided in Table III, sourced from [27].

A. Case Study 1: Open-Loop Performance Without Controller

In order to better illustrate the effectiveness of the proposed method, we firstly discuss the open-loop performance of voltage tracking in this case.

As shown in Fig. 3, without a controller, DCmGs experience significant voltage shocks and oscillations. According to the survey [39], 34% of manufacturers consider power semiconductor devices (e.g., IGBTs or MOSFETs within converters) to

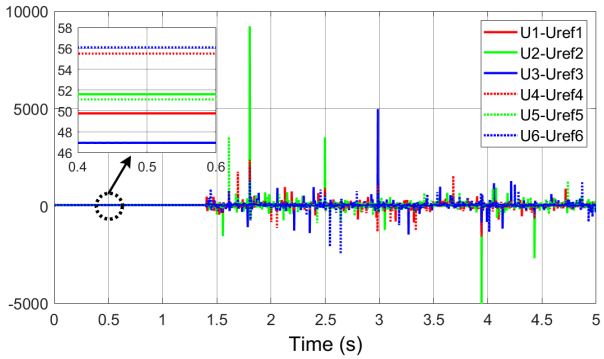

Fig. 3: Voltage tracking at PCCs of the open-loop DCmGs without the controller implementation.

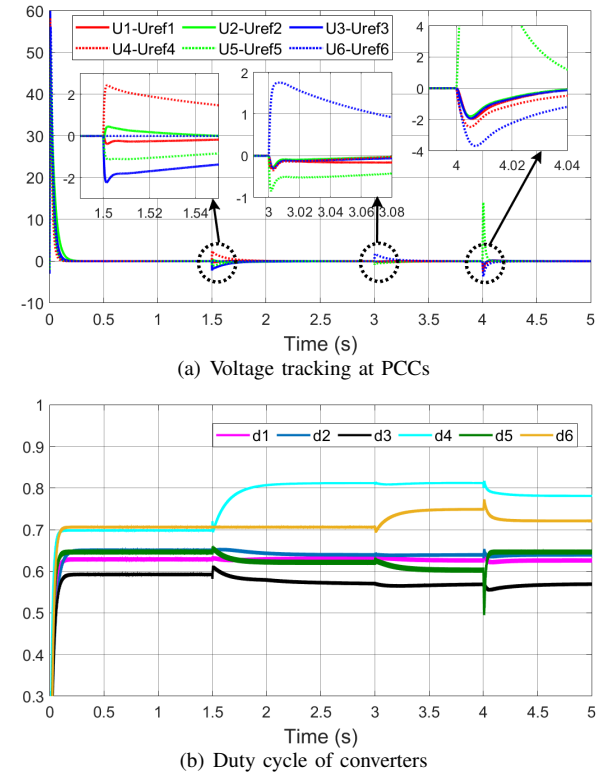

(a) Voltage tracking at PCCs

(b) Duty cycle of converters

Fig. 4: Scalable performance for plugging-in/-out operations.

be the most vulnerable components in their power electronics products. Therefore, such overvoltage events can damage power electronic devices, leading to failures and damage to the DCmG infrastructure.

These observations highlight the need for an advanced control strategy, as detailed in the subsequent case studies, to tackle the challenges posed by PnP operations and varying CPL power demands, thereby preventing significant voltage fluctuations.

B. Case Study 2: Scalable Performance Under PnP Operations

This case evaluates the scalable performance of the proposed control scheme during PnP operations.

Initially, at $t = 0$ s, DGUs 1–6 are initialized with all power lines disconnected, resulting in no power transfer

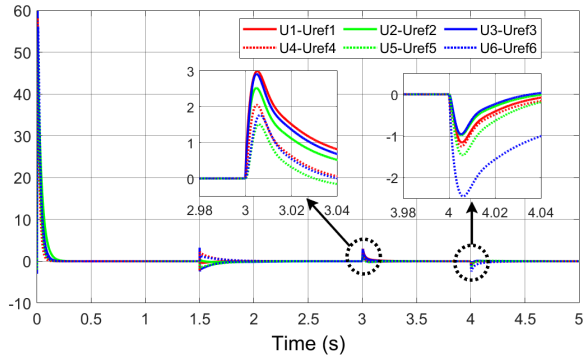

(a) Voltage tracking at PCCs

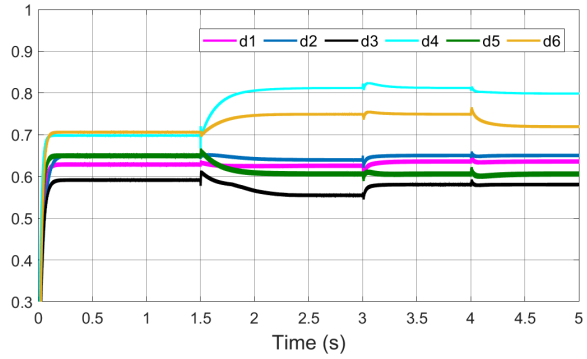

(b) Duty cycle of converters

Fig. 5: Adaptation for increasing/decreasing power of CPLs.

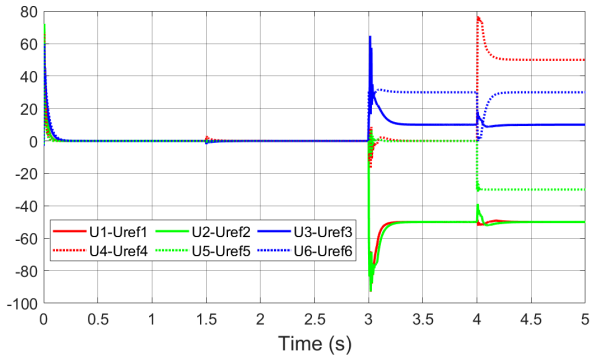

(a) Voltage tracking at PCCs using the control method in [19]

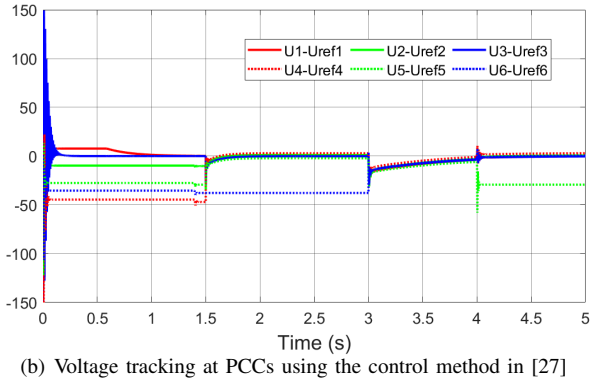

(b) Voltage tracking at PCCs using the control method in [27]

Fig. 6: Comparative analysis with existing control methods.

between them. During this phase, the scalable neural network controllers $u_i(t), i = 1, 2, \ldots, 6$ regulate PCC voltages to their reference values $U_{\text{ref}i}$. At $t = 1.5$ s, DGUs 1–5 are interconnected, forming the DCmG system $\mathbf{S}_5$, while DGU 6 remains disconnected. At $t = 3$ s, DGU 6 is plugged-in, and DGU 5 is unplugged at $t = 4$ s.

As depicted in Fig. 4(a), PCC voltage signals exhibit only minor deviations from their set-point references during PnP operations, with prompt recovery. The control signal is represented as $u_i = d_i U_{si}$, with only the duty cycle d_i shown in Fig. 4(b). These results demonstrate the scalable performance of the proposed voltage controllers during the PnP operations of DGUs with CPLs.

C. Case Study 3: Adaptation to Varying CPL Power Demands

This case assesses the adaptation performance of the proposed control scheme in response to varying CPL power demands.

After the DCmGs are initialized and interconnected, a simulation is conducted where $P_{\ell 1}$ increases to 570W, $P_{\ell 2}$ to 490W, and $P_{\ell 3}$ to 481W at $t = 3$ s. Subsequently, at $t = 4$ s, $P_{\ell 4}$ decreases to 252W, $P_{\ell 5}$ to 240W, and $P_{\ell 6}$ to 195W. The voltage tracking signals at PCCs are depicted in Fig. 5(a), and the corresponding control signals are presented in Fig. 5(b). These results demonstrate that the voltage signals remain close to their reference values, with negligible steady-state error and fast recovery from any deviations. Therefore, the proposed scalable neural network control method effectively adapts to the varying power demands of the CPLs.

D. Case Study 4: Comparative Analysis With Existing Methods

To further validate the proposed approach, comparative simulations are conducted with two representative methods: the robust control strategy in [19], which addresses CPL-induced nonlinearity but lacks PnP capability, and the scalable voltage control method in [27], which supports PnP operations but does not consider CPLs. The initialization and PnP operations in this case follow the same timing sequence as described in case study 2.

The results, shown in Fig. 6(a) and Fig. 6(b), highlight the limitations of these existing methods. Specifically, Fig. 6(a) shows that the method in [19] exhibits significant voltage deviations during PnP operations, which remain uncorrected due to its limited scalability. Meanwhile, Fig. 6(b) indicates that the method in [27] fails to maintain voltage stability under the influence of CPLs, reflecting its inability to address the destabilizing effects of such loads. By contrast, the proposed approach, as illustrated in Fig. 4, effectively addresses these issues in one framework.

VI. Conclusion

This paper proposed a scalable neural network control strategy designed to stabilize voltage in nonlinear DCmGs with CPLs. To address the nonlinearities introduced by CPLs, RBF neural networks were employed, without relying on Lipschitz or bounded conditions. To mitigate the line couplings, a structured Lyapunov matrix was utilized, transforming these effects into a Laplacian structure of the admittance matrix. Furthermore, a scalable neural network control approach was

developed, ensuring scalability for smooth PnP operations and maintaining UUB stability. Case studies on a modified IEEE 37-node test system verified the effectiveness of the proposed approach. Future research will focus on extending this scalable methodology to achieve more advanced control objectives by combining a hierarchical architecture, such as current sharing and voltage balancing in cyber-physical DCmGs.

REFERENCES

[1] L. Ding, Q. -L. Han, L. Y. Wang, and E. Sindi, "Distributed cooperative optimal control of DC microgrids with communication delays," *IEEE Trans. Ind. Inform.*, vol. 14, no. 9, pp. 3924–3935, Sep. 2018.

[2] W. Yao, Y. Wang, Y. Xu, and C. Deng, "Cyber-resilient control of an islanded microgrid under latency attacks and random DoS attacks," *IEEE Trans. Ind. Inform.*, vol. 19, no. 4, pp. 5858–5869, Apr. 2023.

[3] H. Wu, L. Chai, Z. -H. Zhu, and Y. -C. Tian, "Prescribed-time control for DC microgrids with battery energy storage systems," *IEEE Trans. Ind. Inform.*, vol. 20, no. 10, pp. 11896–11907, Oct. 2024.

[4] F. Yang, X. Xie, Q. Sun, and D. Yue, "FDI attack estimation and event-triggered resilient control of DC microgrids under hybrid attacks," *IEEE Trans. Smart Grid*, vol. 15, no. 4, pp. 4207–4216, Jul. 2024.

[5] Y. Yu, G. -P. Liu, Y. Huang, and J. M. Guerrero, "Coordinated predictive secondary control for DC microgrids based on high-order fully actuated system approaches," *IEEE Trans. Smart Grid*, vol. 15, no. 1, pp. 19–33, Jan. 2024.

[6] C. Deng, F. Guo, C. Wen, D. Yue, and Y. Wang, "Distributed resilient secondary control for DC microgrids against heterogeneous communication delays and DoS attacks," *IEEE Trans. Ind. Electron.*, vol. 69, no. 11, pp. 11560–11568, Nov. 2022.

[7] M. Kumar, S. C. Srivastava, and S. N. Singh, "Control strategies of a DC microgrid for grid connected and islanded operations," *IEEE Trans. Smart Grid*, vol. 6, no. 4, pp. 1588–1601, Jul. 2015.

[8] B. Xia, S. Fan, L. Ding, and C. Deng, "Distributed dynamic event-triggered resilient control for AC microgrids under FDI attacks," *IEEE Trans. Circuits Syst. I-Regul. Pap.*, vol. 71, no. 3, pp. 1406–1416, Mar. 2024.

[9] B. Ning, Q. -L. Han, and L. Ding, "Distributed finite-time secondary frequency and voltage control for islanded microgrids with communication delays and switching topologies," *IEEE Trans. Cybern.*, vol. 51, no. 8, pp. 3988–3999, Aug. 2021

[10] T. Dragičević, X. Lu, J. C. Vasquez, and J. M. Guerrero, "DC microgrids-Part I: A review of control strategies and stabilization techniques," *IEEE Trans. Power Electron.*, vol. 31, no. 7, pp. 4876–4891, Jul. 2016.

[11] R. Samsami, H. Mirshekali, R. Dashti, M. M. Arefi, and H. R. Shaker, "Robust model predictive control of uncertain DC microgrids based on improved adaptive consensus algorithm," *IEEE Trans. Ind. Inform.*, vol. 20, no. 11, pp. 13486–13497, Nov. 2024.

[12] X. Li, X. Zhang, W. Jiang, J. Wang, P. Wang, and X. Wu, "A novel assorted nonlinear stabilizer for DC-DC multilevel boost converter with constant power load in DC microgrid," *IEEE Trans. Power Electron.*, vol. 35, no. 10, pp. 11181–11192, Oct. 2020.

[13] A. C. Braitor, G. Konstantopoulos, and V. Kadirkamanathan, "Stability analysis of DC micro-grids with CPLs under novel decentralized primary and distributed secondary control," *Automatica*, vol. 139, May 2022, Art. no. 110187.

[14] S. Bahrami, S. S. Mousavi, and M. Shafiee-Rad, "Decentralized adaptive nonlinear controller for voltage regulation of output-constrained DC microgrids with ZIP loads," *IEEE Trans. Power Syst.*, vol. 39, no. 5, pp. 6210–6221, Sep. 2024.

[15] F. Boem, R. Carli, M. Farina, G. Ferrari-Trecate, and T. Parisini, "Distributed fault detection for interconnected large-scale systems: A scalable plug & play approach," *IEEE Trans. Control Netw. Syst.*, vol. 6, no. 2, pp. 800–811, Jun. 2019.

[16] C. Chen and S. Duan, "Optimal integration of plug-in hybrid electric vehicles in microgrids," *IEEE Trans. Ind. Inform.*, vol. 10, no. 3, pp. 1917–1926, Aug. 2014.

[17] I. Kouveliotis-Lysikatos, D. I. Koukoula, A. L. Dimeas, and N. D. Hatziargyriou, "Plug-and-play algorithms for the efficient coordination of active distribution grids," *Proc. IEEE*, vol. 110, no. 12, pp. 1927–1939, Dec. 2022.

[18] J. Su, K. Li, and C. Xing, "Plug-and-play of grid-forming units in DC microgrids assisted with power buffers," *IEEE Trans. Smart Grid*, vol. 15, no. 2, pp. 1213–1226, Mar. 2024.

[19] S. Hu, P. Yuan, D. Yue, C. Dou, Z. Cheng, and Y. Zhang, "Attack-resilient event-triggered controller design of DC microgrids under DoS attacks," *IEEE Trans. Circuits Syst. I-Regul. Pap.*, vol. 67, no. 2, pp. 699–710, Feb. 2020.

[20] D. Zonetti, R. Ortega, and J. Schiffer, "A tool for stability and power-sharing analysis of a generalized class of droop controllers for high-voltage direct-current transmission systems," *IEEE Trans. Control Netw. Syst.*, vol. 5, no. 3, pp. 1110–1119, Sep. 2018.

[21] X. Xu, Q. Liu, C. Zhang, and Z. Zeng, "Prescribed performance controller design for DC converter system with constant power loads in DC microgrid," *IEEE Trans. Syst. Man Cybern. -Syst.*, vol. 50, no. 11, pp. 4339–4348, Nov. 2020.

[22] J. Liu, W. Zhang, and G. Rizzoni, "Robust stability analysis of DC microgrids with constant power loads," *IEEE Trans. Power Syst.*, vol. 33, no. 1, pp. 851–860, Jan. 2018.

[23] F. Yang, X. Xie, and C. Peng, "Co-design of new fuzzy switching-type state-FDI estimation and attack compensation for DC microgrids under hybrid attacks," *IEEE Trans. Fuzzy Syst.*, vol. 32, no. 4, pp. 1743–1755, Apr. 2024.

[24] L. Herrera, W. Zhang, and J. Wang, "Stability analysis and controller design of DC microgrids with constant power loads," *IEEE Trans. Smart Grid*, vol. 8, no. 2, pp. 881–888, Mar. 2017.

[25] A. Wang, M. Fei, and Y. Song, "A novel scalable and reliable control for DC microgrids with varying number of agents," *IEEE Trans. Cybern.*, vol. 54, no. 9, pp. 4962–4972, Sep. 2024.

[26] M. S. Sadabadi, Q. Shafiee, and A. Karimi, "Plug-and-play robust voltage control of DC microgrids," *IEEE Trans. Smart Grid*, vol. 9, no. 6, pp. 6886–6896, Nov. 2018.

[27] M. Tucci, S. Riverso, and G. Ferrari-Trecate, "Line-independent plug-and-play controllers for voltage stabilization in DC microgrids," *IEEE Trans. Control Syst. Technol.*, vol. 26, no. 3, pp. 1115–1123, May 2018.

[28] A. Wang, M. Fei, D. Du, and Y. Song, "A novel scalable fault-tolerant control design for DC microgrids with nonuniform faults," *IEEE/CAA J. Autom. Sinica*, vol. 11, no. 8, pp. 1886–1888, Aug. 2024.

[29] V. Venkatasubramanian, H. Schattler, and J. Zaborszky, "Fast time-varying phasor analysis in the balanced three-phase large electric power system," *IEEE Trans. Autom. Control*, vol. 40, no. 11, pp. 1975–1982, Nov. 1995.

[30] *IEEE Recommended Practice for Monitoring Electric Power Quality*, IEEE Standard 1159, 2009.

[31] F. Dörfler and F. Bullo, "Kron reduction of graphs with applications to electrical networks," *IEEE Trans. Circuits Syst. I-Regul. Pap.*, vol. 60, no. 1, pp. 150–163, Jan. 2013.

[32] Z. Feng, R. -B. Li, and L. Wu, "Adaptive decentralized control for constrained strong interconnected nonlinear systems and its application to inverted pendulum," *IEEE Trans. Neural Netw. Learn. Syst.*, vol. 35, no. 7, pp. 10110–10120, Jul. 2024.

[33] A. Wang, M. Fei, Y. Song, D. Du, C. Peng, and K. Li, "Scalable fuzzy control for nonlinear DC microgrids under plug-and-play operations," *IEEE Trans. Fuzzy Syst.*, vol. 32, no. 8, pp. 4747–4758, Aug. 2024.

[34] A. Wang, M. Fei, Y. Song, C. Peng, D. Du, and Q. Sun, "Secure adaptive event-triggered control for cyber-physical power systems under denial-of-service attacks," *IEEE Trans. Cybern.*, vol. 54, no. 3, pp. 1722–1733, Mar. 2024.

[35] H. Khalil. *Nonlinear Systems (3rd ed.)*. Prentice Hall, 2002.

[36] D. K. Fulwani and S. Singh, *Mitigation of Negative Impedance Instabilities in DC Distribution Systems-A Sliding Mode Control Approach*. Berlin, Germany: Springer, 2016.

[37] N. Vafamand, M. H. Khooban, T. Dragičević, F. Blaabjerg, and J. Boudjadar, "Robust non-fragile fuzzy control of uncertain DC microgrids feeding constant power loads," *IEEE Trans. Power Electron.*, vol. 34, no. 11, pp. 11300–11308, Nov. 2019.

[38] A. C. Rueda-Medina and A. Padilha-Feltrin, "Distributed generators as providers of reactive power support-A market approach," *IEEE Trans. Power Syst.*, vol. 28, no. 1, pp. 490–502, Feb. 2013.

[39] S. Yang, A. Bryant, P. Mawby, D. Xiang, L. Ran, and P. Tavner, "An industry-based survey of reliability in power electronic converters," *IEEE Trans. Ind. Appl.*, vol. 47, no. 3, pp.1441–1451, May/Jun. 2011.